Atmospheric Environment 142 (2016) 57–70

Contents lists available at ScienceDirect

Atmospheric Environment

journal homepage: www.elsevier.com/locate/atmosenv

Deriving aerosol hygroscopic mixing state from size-resolved CCN activity and HR-ToF-AMS measurements

Deepika Bhattu [a], S.N. Tripathi [a, b, *], Abhishek Chakraborty [a]

[a] Department of Civil Engineering, Centre for Environmental Science & Engineering, Indian Institute of Technology Kanpur, Uttar Pradesh, India
[b] Department of Earth Sciences, Indian Institute of Technology Kanpur, Uttar Pradesh, India

HIGHLIGHTS

- Accumulation mode particles are more hygroscopic and homogeneously mixed compared to Aitken mode.
- κ_{AMS} is over-predicted compared to κ_{CCN} as organic and inorganic mass in Aitken mode is not appropriately approximated by bulk composition.
- Increased deviation of ~100% between κ_{CCN} and κ_{AMS} due to sudden influx of freshly emitted BBOA caused suppressed hygroscopic growth.

ARTICLE INFO

Article history:
Received 20 January 2016
Received in revised form
6 July 2016
Accepted 12 July 2016
Available online 16 July 2016

Keywords:
Accumulation
Aitken mode
Hygroscopic
CCN-inactive
Chemically-resolved

ABSTRACT

The ability of a particle to uptake water and form a cloud droplet depends on its hygroscopicity. To understand its impact on cloud properties and ultimately radiative forcing, knowledge of chemically-resolved mixing state information or the one based on hygroscopic growth is crucial. Typically, global models assume either pure internal or external mixing state which might not be true for all conditions and sampling locations. To investigate into this, the current study employed an indirect approach to infer the probable mixing state. The hygroscopic parameters derived from κ-Kohler theory using size-resolved CCN measurements (κ_{CCN}) and bulk/size-resolved aerosol mass spectrometer (AMS) measurements (κ_{AMS}) were compared. The accumulation mode particles were found to be more hygroscopic ($\kappa_{CCN} = 0.24$) than Aitken mode ($\kappa_{CCN} = 0.13$), perhaps due to increased ratio of inorganic to organic mass fraction. The activation diameter calculated from size-resolved CCN activity measurements at 5 different supersaturation (SS) levels varied in the range of 115 nm–42 nm with $\kappa_{CCN} = 0.13–0.23$ (avg $= 0.18 \pm 0.10$ ($\pm 1\sigma$)). Further, $\kappa_{AMS} > \kappa_{CCN}$ was observed possibly due to the fact that organic and inorganic mass present in the Aitken mode was not correctly represented by bulk chemical composition and size-resolved fractional contribution of oxidized OA was not accurately accounted. Better correlation of organic fraction (f_{org}) and κ_{CCN} at lower SS explained this behaviour. The decrease in κ_{CCN} with the time of the day was more pronounced at lower SS because of the relative mass reduction of soluble inorganic species by ~17%.

Despite the large differences between κ measured from two approaches, less over-prediction (up to 18%) between measured and predicted CCN concentration suggested lower impact of chemical composition and mixing state at higher SS. However, at lower SS, presences of externally mixed CCN-inactive aerosols lead to CCN over-prediction reflecting the significance of aerosol mixing state information. Further examination of the effect of biomass burning aerosols (~35% in least oxidized biomass burning organic aerosol (BBOA-2 fraction) on hygroscopicity and CCN activity showed increase in the concentration of all AMS measured species (except NH_4^+ and SO_4^{2-}), less O:C ratio, and organic mass fraction (f_{org}) peak shift to lower diameter range caused ~13% change in critical diameter (D_a) and ~40% change in κ_{CCN}. Increased deviation of ~100% between κ_{CCN} and κ_{AMS} due to sudden influx of internally mixed BBOA caused suppressed hygroscopic growth. This study finally suggests the assumption of pure internally mixed aerosol does not completely hold true for this anthropogenically polluted site.

1. Introduction

Atmospheric aerosols can act as cloud condensation nuclei

* Corresponding author: Department of Civil Engineering, Centre for Environmental Science & Engineering, Indian Institute of Technology Kanpur, Uttar Pradesh, India.
E-mail address: snt@iitk.ac.in (S.N. Tripathi).

http://dx.doi.org/10.1016/j.atmosenv.2016.07.032
1352-2310/

(CCN), depending on their size, chemical composition, and mixing state, and affect the microphysical properties, lifetime, and coverage area of clouds by altering the size and number concentration of cloud droplets (Bauer and Menon, 2012; Farmer et al., 2015; Stocker et al., 2013). Precise quantification of CCN concentration is required when aerosol activation fraction (CCN/CN) is non-linearly linked to the total aerosol concentration (CN) and involves complexity due to various atmospheric processes affecting their mixing state (Anttila et al., 2012). Their existence in the form of internally (same dry size with same chemical composition) or externally (same dry size with different chemical composition) mixed particles and further climatic impacts depend on several factors. These factors include the distance from the source, location, and evolution processes, transition of the initial hydrophobic component, like freshly emitted black carbon (BC) to hydrophilic due to coagulation or condensation of soluble species. For example, the impact of BC absorption on radiative forcing increases by a factor of 2.9 when shifted from externally mixed to internally mixed aerosols (Jacobson, 2001). In addition to such extreme scenarios, a recent study demonstrated the changes in direct radiative forcing due to morphological modifications and absorption enhancement (factor of 2.4) depending on the rate and timescale of BC aging (Peng et al., 2016).

Apart from the particle number, size, and chemical composition, the aerosol mixing state is an important parameter affecting cloud activation processes and deciding the cloud droplet activation fraction in polluted regions. The assumption of purely internally or externally mixed aerosols over-estimate or under-estimate the CCN concentration and contribute up to an error of ~40% in CCN prediction. Especially in the regions with high primary organic aerosols (POA) and BC mass fractions (mainly during traffic hours or biomass burning events) (Lance et al., 2013; Wang et al., 2010). However, its impact on achieving the CCN closure with <10% deviation from measured CCN concentration reduces with the increase in soluble organic fraction or in cases with effective hygroscopicity, $\kappa > 0.1$. Thus, site-specific long-term comprehensive field studies focusing deliberately on mixing state are required to reduce both over- and under-prediction of CCN concentration and incorporate the outcome in regional climate models (Spracklen et al., 2008).

A hygroscopicity parameter (Petters and Kreidenweis, 2007) representing the water uptake capacity of aerosols can be derived from hygroscopic growth factor, CCN activity or chemical composition measurements. These growth measurements provide information on aerosol mixing state with respect to the hygroscopicity. In the past, few laboratory and ambient studies have focussed on the influence of mixing state on size-resolved CCN spectra with more emphasis on internally mixed aerosols (Dusek et al., 2010). Hygroscopicity distributions from HTMDA (Fors et al., 2011) and size-resolved CCN measurements (Gunthe et al., 2009; Rose et al., 2010) have been used to infer mixing state and understand the processes affecting hygroscopic growth (Gunthe et al., 2009; Mochida et al., 2010). Several measurement techniques, such as scanning and transmission electron microscope (STEM) (Adachi and Buseck, 2008; Pöschl et al., 2010), single particle mass spectrometers (SPMS) (Murphy et al., 2006), and tandem differential mobility analyser (TDMA) (McMurry et al., 1996) have shown the existence of variation in the degree of mixing state with particle size in ambient atmosphere. So, reporting bulk κ values assuming only internally mixed aerosols may not always describe the real impact of the hygroscopicity distributions on CCN prediction (Wang et al., 2010).

In this work, we have derived κ using both bulk and size-resolved chemical composition data from AMS (κ_{AMS}), and size-resolved CCN measurements (κ_{CCN}), separately. κ_{AMS} and κ_{CCN} are then compared with each other. Based on the results of this hygroscopicity closure, we have attempted to infer the probable size-resolved aerosol mixing state. The effect of chemical composition and solubility of organics on CCN activity at different SS levels is also examined. Further, a case study has been done to investigate the effect of biomass burning aerosols on physical (size distribution and mixing state) and chemical aerosol properties.

2. Methods

2.1. Site description

Measurements of physico-chemical properties and CCN activity of ambient aerosol were carried out from 1 to 20 December 2012 at the Centre for Environmental Science and Engineering (CESE) in Indian Institute of Technology (IIT) Kanpur campus. Temperature and relative humidity (RH) ranges from 11.2 to 25.7 °C and 18.7–81.1% with mean ± 1SD of 18.7 ± 3.5 °C and 50.7 ± 14.5%, respectively during the study period. The major pollution sources at this site in winter season are vehicular emissions, industrial emissions, freshly emitted and long range transported biomass burning aerosols, waste (such as garbage and leaf litter) burning,, and domestic cooking (Bhattu and Tripathi, 2015; Garg et al., 2016; Kanawade et al., 2014; Nandy et al., 2015). A large number of emission sources and high aerosol loading conditions pose a challenge in unravelling the complex aerosol properties. Further, three days backward trajectory cluster analysis at 500 m above mean sea level was performed using HYSPLIT 4.8 model (Supplementary section S1 and Fig. S1).

2.2. Instrumentation and data collection

Ambient air was passed through a silica gel diffusional dryer (outlet RH < 30%) before entering to the instruments connected further. Three lines were separated, out of which one passed to the Aerodyne HR-ToF-AMS (hereafter AMS) to measure the bulk and size-resolved chemical composition, another to scanning mobility particle sizer (SMPS, TSI3696) to measure the total aerosol number-size distribution with scan time of 120 s ($dN/dlogD_p$), and the third to differential mobility analyser (DMA, TSI3081, sheath to aerosol ratio = 10:1, sample flow = 0.8 lpm). This was further connected to condensation particle counter (CPC, TSI 3776, sample flow = 0.3 lpm) and cloud condensation nuclei counter (CCNc, DMT-100, sheath to aerosol ratio = 10:1, sample flow = 0.5 lpm) in parallel to count the size-selected total aerosol concentration (cm^{-3}) and CCN concentration (cm^{-3}), respectively. The activation fraction (CCN/CN) of these size-selected particles was measured at 5 different supersaturation (SS) levels (0.2, 0.3, 0.5, 0.8, and 1.2%). SS calibration was done at 6 column temperature differences, ΔT (2 K, 4 K, 8 K, 12 K, 16 K and 18 K) using pure mono-dispersed ammonium sulfate aerosols (purity > 99%, Fischer Scientific) (Fig. S4). The calibration procedure and effective SS calculations were performed by following the method explained in Rose et al. (2008). For each SS measurement cycle, a maximum of 17 particle diameters (residence time of 2 min at each diameter) ranging from 20 to 280 nm were selected depending on the SS applied. One complete cycle of CCN efficiency spectra measurement at 5 SS levels was completed in ~164–172 min (~30–34 min at each SS; including 6 min interval when shifting from higher to lower SS and 2 min at every alternate SS). The data integration time at each size was kept to be 60 s while discarding every initial 60 s data. Each day 4 sets of complete cycle of CCN efficiency spectra were measured (Phase I: 0900–1200 h, Phase II: 1300–1600 h, Phase III: 1600–1900 h, and Phase IV: 2000–2300 h). Due to low sampling frequency, daily data was resolved into four phases to understand the effect of diurnal

variation of atmospheric conditions like RH, temperature, and boundary layer, and chemical composition on CCN activity. Total 360 CCN efficiency spectra (72 at each SS) were collected during the whole sampling period. Except, AMS all the other instruments were operated from 0900 h to 2300 h.

The ambient relative humidity and temperature were measured using a temperature and RH sensor (Vaisala, Inc. Humicap, HMT337 accuracy of ±1% for RH < 90%). To obtain chemical composition, AMS was operated alternatively in V and W mode at a vaporizer temperature of 600 °C, each with 1 min averaging time. Details on AMS and its operation are given elsewhere (Bhattu and Tripathi, 2015; DeCarlo et al., 2006). It samples the sub-micron particles with vacuum aerodynamic diameter of 60–700 nm with 100% transmission efficiency. It measures the non-refractory species like total organic mass concentration, ammonium, nitrate, sulfate, and chloride (μg m^{-3}). AMS was calibrated for ionization efficiency (IE) i.e., number of ions measured from a known amount of mass using size-selected NH_4NO_3 aerosols (350 nm) from different concentrated solutions. A mass balance approach is then used to calculate the IE and RIE of NH_4^+ w.r.t. NO_3^-. Relative ionization efficiency (RIE) for organics, SO_4^{2-}, NO_3^-, and Cl^- was assumed to be 1.4, 1,2, 1.1, and 1.3, and for NH_4^+, RIE of 4.6 was calculated during IE calibration (Chakraborty et al., 2015). The organic aerosol density was found to be 1.3 kg/m^3 using O:C and H:C ratios (Kuwata et al., 2012) and the fractional contribution of three components ($(NH_4)_2SO_4$, NH_4NO_3, and organics) was used to calculate the effective particle density (ρ_{eff}). The limit of detection, defined as the 3 times the standard deviations of species concentration values in particle free air (DeCarlo et al., 2006) was found to be 153, 24, 36, 45, and 12 ng/m^3 for organics, NO_3^-, SO_4^{2-}, NH_4^+, and Cl^-. The chemically dependent collection efficiency (CDCE) of 0.45 is used in this study based on the calculations depending on the amount of NO_3^- and SO_4^{2-} collected (Bhattu and Tripathi, 2015; Middlebrook et al., 2011).

3. Data processing

3.1. Size-resolved CCN activity

The CCN efficiency spectra (CCN/CN) at SS = 0.2–1.2% were fitted using Cumulative Distribution Function (CDF) fit given in equation (1) (Rose et al., 2008) after multiple charge correction (Frank et al., 2006) and DMA transfer function correction (Frank et al., 2006; Petters et al., 2007).

$$f_{\frac{CCN}{CN}} = a\left(1 + erf\left(\frac{D - D_a}{\sigma_a\sqrt{2}}\right)\right) \quad (1)$$

where, a and σ_a are fitting parameters of 3-parameter CDF fit representing half of the maximum activated fraction (MAF = 2a) and standard deviation of the fit, respectively. D_a is the activation diameter at which 50% of the total particles get activated (i.e. a = 0.5) and MAF = 1. Further details on CDF parameters and calculations of hygroscopicity are given in Supplementary section (S3 and S4).

3.2. PMF analysis

The aerosol chemical composition (bulk and size-resolved) was measured by AMS (DeCarlo et al., 2006). The software package Igor Pro 6.34 A (Wavemetrices) was used for data analysis (SQUIRREL 1.54A, PIKA 1.13A) (Sueper et al., 2007). Positive matrix factorization (PMF; Evaluation Tool v2.06) analysis of high-resolution (HR) mass spectra (m/z 12–300, V mode) was done to identify the different sources of organic aerosols (Ulbrich et al., 2009) (Fig. S2 a-i). A six-factor solution (fPeak = 0) was chosen to be the optimal solution on the basis of factor profiles, the correlation between factor profiles, and time series, and their relationship with the external factors. More details on factor analysis are given in the supplementary section S2.

3.3. CCN closure

In CCN closure approach, CCN concentration predicted from Köhler theory using was compared with the measured concentration. The measured CCN concentrations at different SS conditions were calculated by integrating the CCN size distribution over the full measured size range. CCN size distribution ($dCCN/dlogD_p$) was obtained by multiplying the CCN activated fraction (CCN/CN) with the CN size distribution ($dCN/dlogD_p$) measured in parallel.

In this study, different combinations of size-resolved and bulk composition with their solubility were chosen for CCN prediction. The four cases considered in this study were: (i) size-resolved chemical composition with all organics assumed to be soluble (SR-ALLORG-SOL); (ii) size-resolved chemical composition with LVOOA assumed to be the only soluble species among organics (SR-LV-SOL); (iii) bulk chemical composition with all organics assumed to be soluble (BULK-ALLORG-SOL); and (iv) bulk chemical composition with LVOOA assumed to be only soluble species among organics (BULK-LV-SOL). Further, procedure on the calculations of organic density, critical diameter and predicted CCN concentration is given in Supplementary section S5. In size-resolved composition scenario, the soluble organic fraction was obtained by multiplying the relative contribution of LVOOA in the bulk organics with the mass size distribution of organics obtained from AMS. The calculation scheme used here is same as given in section 2.2. of Bhattu and Tripathi (2015). As this approach lacks the information on size-resolved O:C ratio which has larger effect on actual WSOC concentration, it can also add to the deviation in hygroscopicity closure (κ_{CCN} and κ_{AMS}). The aerosols were assumed to be internally mixed in nature. To minimize the uncertainties involved due to assumptions like bulk or size-resolved composition and solubility of organics, hygroscopicity parameter was calculated only for the cases with better proximity between CCN measured and predicted. κ_{AMS} was calculated for these pairs of SS and D_c using κ-Köhler theory (equation S(1)). κ_{AMS} was calculated even for the data points with SNR equal to 2 in order to provide the approximate differences between κ_{AMS} and κ_{CCN}.

4. Results and discussion

4.1. Time series of aerosol properties

Fig. 1 (a, c, e, g) shows the time series of RH (%) and temperature (°C), aerosol size distribution, mass fraction of organic PMF factors (BBOA-3, LVOOA, BBOA-1, SVOOA, BBOA-2, and HOA), NH_4NO_3, $(NH_4)_2SO_4$ mass concentrations and κ_{CCN} derived at different SS levels. The gaps in the data points are due to general maintenance and non-availability of the instruments. The minimum and maximum temperature observed during the sampling period were 11.2 °C and 25.7 °C (with a mean ± standard deviation of 18.7 ± 3.5 °C). RH ranged from 18.7% to 81.2% (50.7± 14.5%) (Fig. 1a). The total aerosol number concentration varied between 4000 and 58000 cm^{-3} with a maxima during morning and evening hours due to traffic emissions and lower boundary layer height, and minima during daytime due to dilution with the increase in boundary layer height (Fig. 1c, d). On an average, the particle mode diameter ranged between 70 nm and 140 nm.

The concentration of organics, $(NH_4)_2SO_4$ and NH_4NO_3 varied from 6 to 123 μg m^{-3} (avg ± 1std = 45.0 ± 25.6), 2–22.7 μg m^{-3} (8.4 ± 3.7) and 1–42.4 μg m^{-3} (13.3 ± 8.68), respectively, during the

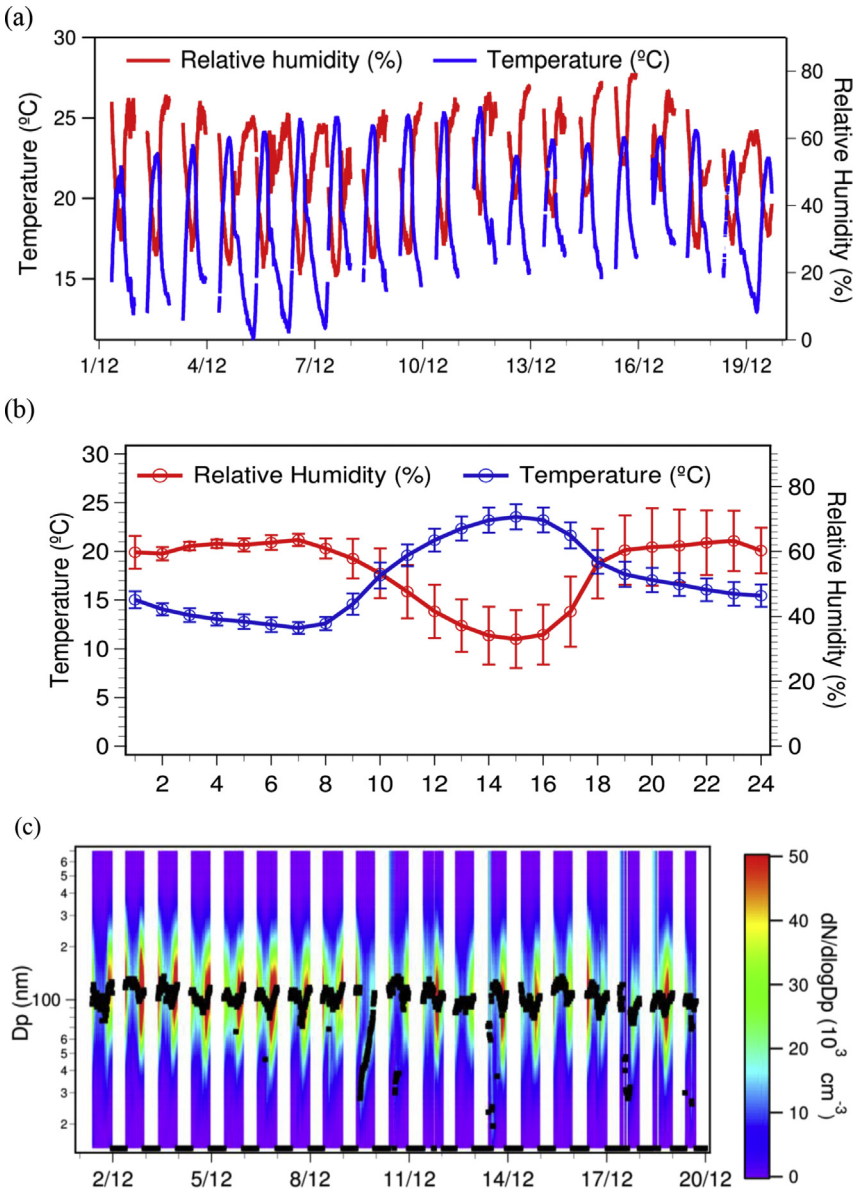

Fig. 1. Time series and diurnal variation of (a,b) RH and temperature; (c, d) aerosol size distribution; (e, f) PMF factors mass fraction; (g, h) Organics, NH_4NO_3 and $(NH_4)_2SO_4$ mass fraction, and NH_4NO_3 and $(NH_4)_2SO_4$ mass concentrations; (i) κ_{CCN} (Here, Phase I, II, III, and IV are represented as 1,2,3, and 4; Just to guide the eye, data points at all SS are offset by 0.1).

sampling period. Organics (~66.5%) were found to be the major constituent of total non-refractory submicron aerosol mass measured by the AMS. $(NH_4)_2SO_4$ and NH_4NO_3 constituted ~14.5% and ~19% of the total mass, respectively (Fig. 1g).

Among the organics, LVOOA had the maximum average concentration (13.38 μg m^{-3}; 35% of total organics) followed by BBOA-2 (9.39 μg m^{-3}; 16%), SVOOA (6.33 μg m^{-3}; 14%), HOA (5.86 μg m^{-3}; 12%), BBOA-1 (5.30 μg m^{-3}; 12%), and BBOA-3 (4.81 μg m^{-3}; 10%), respectively (Fig. 1e). LVOOA showed the highest concentration during daytime (1000 h onwards) because of its photochemical production and was associated with a decrease in rest of the factors suggesting their conversion to more oxidized and less volatile form i.e. LVOOA (Fig. 1f). Its production was counteracted by the dilution due to increased mixing layer height leading to less diurnal variation. Similar to LVOOA, the most oxidized fraction among BBOA, i.e., BBOA-3 also showed least diurnal variation suggesting either the conversion of less oxidized BBOA forms (BBOA-1 and 2) to BBOA-3 or presence of long range transported biomass burning aerosols. On the other hand, BBOA-1 and HOA showed the same strong diurnal pattern with O:C ratio of 0.45 and 0.24, respectively, indicating their concurrent emission. The mass fraction of BBOA-2 was found to be higher (0.30–0.35) during the morning (before 0900 h) and evening hours (after 2000 h), which is possibly due to the local use of local conventional fuels in cooking and heating the houses during the winter season. The BBOA-3 contribution increased from 0.09 to 0.18 after Dec. 16 due to increased contribution of long range transported BBOA (from backtrajectory cluster analysis, supplementary section S1) or could be due to oxidative conversion of BBOA-2. Higher vehicular emission caused more HOA fraction (O:C ratio = 0.24) that retained till 2200 h whereas locally emitted BBOA-2 (O:C ratio = 0.27) increased only till midnight.

The fractional mass contribution of $(NH_4)_2SO_4$ varied from 0.10 to 0.25 as the day progressed with maxima in the daytime (between 1500 and 1700 h) (Fig. 1g). The diurnal trend of $(NH_4)_2SO_4$

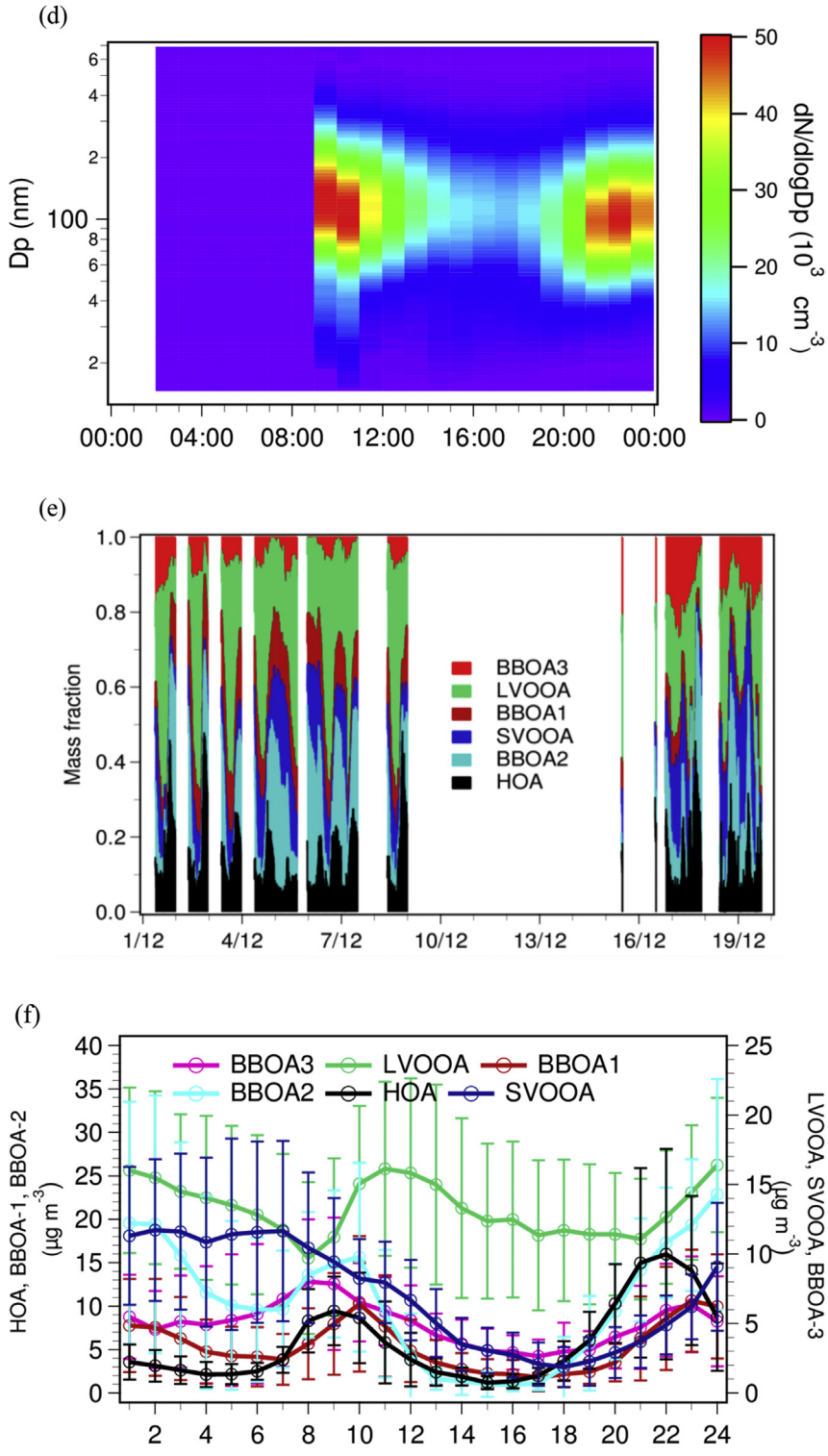

Fig. 1. (*continued*).

showed a peak similar to LVOOA with a time lag in LVOOA production suggesting different formation mechanisms (Fig. 1h) (Bhattu and Tripathi, 2015; Sun et al., 2011). However, increase in NH_4NO_3 concentration during nighttime could be due to the production of NO_3 radical from NO_2 and O_3, which further gets converted to HNO_3 via thermal equilibrium with N_2O_5 (Dall'Osto et al., 2009). The conditions of high RH and low temperature in this study at night were favourable for gas-to-particle conversion of HNO_3.

Depending on the better correlation between measured and predicted CCN concentration (see section 3.4 and 4.4), "κ_{AMS}" was calculated using activation diameter obtained in SR-LVSOL scenarios. The calculated average κ_{AMS} value of 0.28 (1SD = ±0.11 with f_{org}, organic fraction: 66.5%) was observed to be higher than our previous study (κ = 0.20 and 0.12 at day and night), when f_{org} was

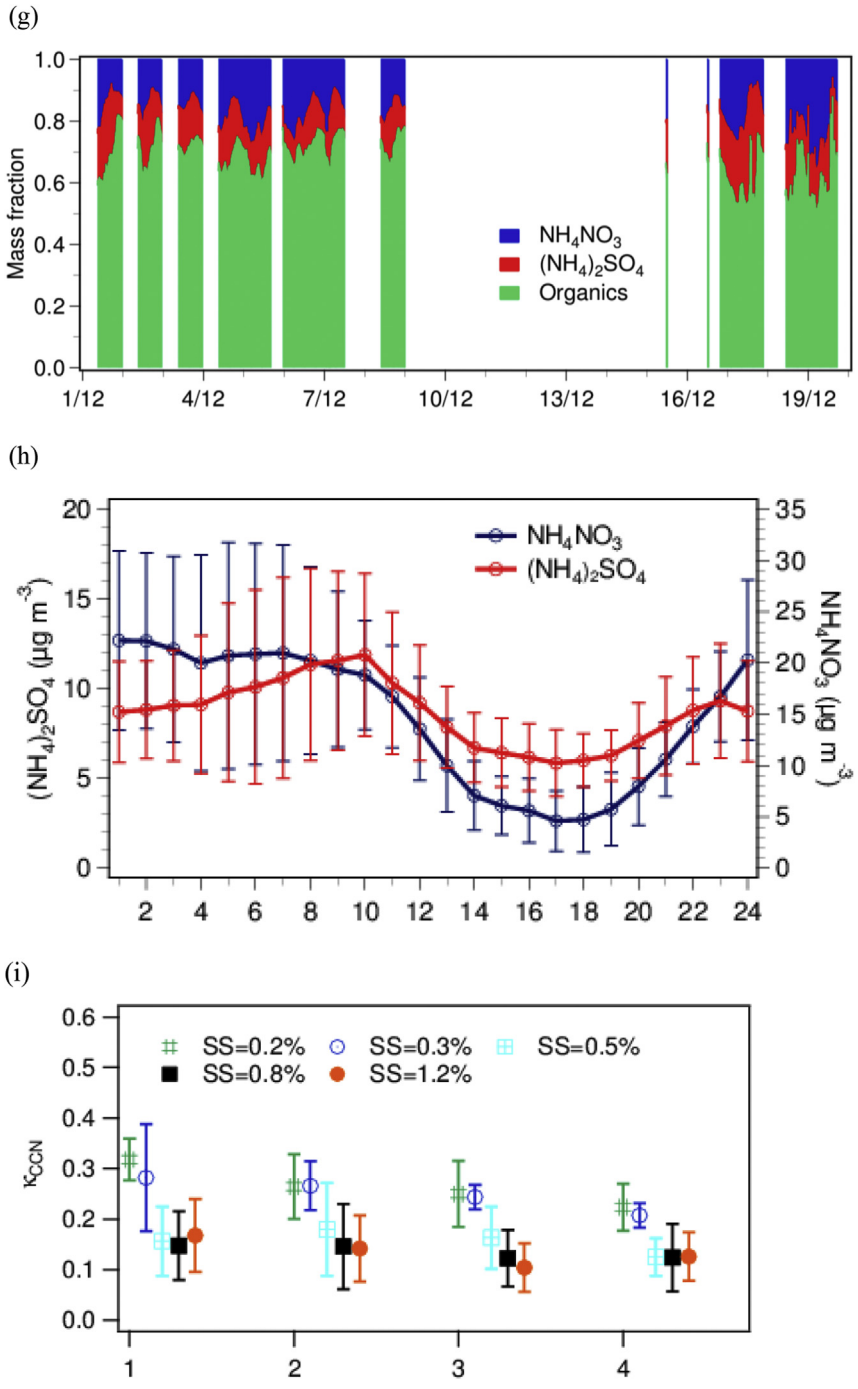

Fig. 1. (*continued*).

~75% (Bhattu and Tripathi, 2015). The maximum variation (~28%) in κ_{AMS} was observed for lower SS suggesting more pronounced effect of chemical composition, i.e., solute effect compared to higher SS.

4.2. CDF parameters and hygroscopicity parameter (κ)

Table 1 shows the average CDF parameters (D_a, σ_a, σ_a/D_a) calculated for the whole sampling data. Here, the average activation diameter (D_a) decreased with increase in SS ranging from ~115 nm to 42 nm at SS = 0.2–1.2%. Fig. 2 demonstrates that all the CCN efficiency spectra reached unity at highest diameter measured suggesting that all the particles were CCN-active in nature. Various past studies have shown the applicability of size-resolved CCN measurements in determining the probable mixing state (Jurányi et al., 2013; Lance et al., 2013; Rose et al., 2013; Wu et al., 2013).

For particles >60 nm, the average σ_a/D_a declined with the decrease in SS suggesting that bigger particles were more homogeneously mixed (Table 1). Table 2 shows the similar results obtained by other previous size-resolved CCN studies (Gunthe et al., 2009, 2011; Rose et al., 2013). However, particles <60 nm were again found to have higher σ_a/D_a suggesting the presence of size-resolved heterogeneity. This could be explained by the possible co-existence of primary particles (Average BC concentration: 8–10 μg m^{-3} Fig. S2g) and processed organic and inorganic

Table 1
Average CDF parameters (D_a, σ_a, σ_a/D_a, κ) calculated from size-resolved CCN measurements.

SS(%)	D_a	σ_a	σ_a/D_a	κ	CCN/CN	n
0.2	115.43 ± 12.55	18.94 ± 10.14	0.16 ± 0.07	0.23 ± 0.07	0.33	70
0.3	84.32 ± 10.57	14.54 ± 6.34	0.17 ± 0.08	0.24 ± 0.06	0.48	51
0.5	77.92 ± 12.21	14.49 ± 7.29	0.18 ± 0.07	0.13 ± 0.06	0.71	73
0.8	58.18 ± 15.71	14.70 ± 15.26	0.22 ± 0.18	0.14 ± 0.07	0.85	72
1.2	42.88 ± 7.10	7.23 ± 4.89	0.16 ± 0.10	0.13 ± 0.06	0.94	73

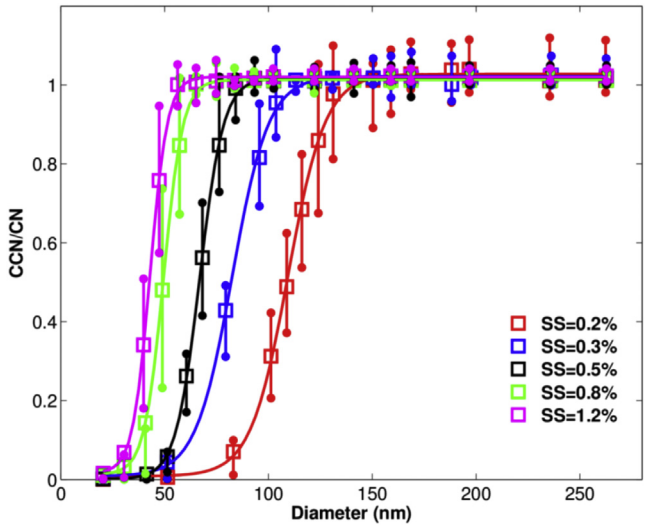

Fig. 2. Averaged size-resolved activation fraction (CCN/CN) measured at different SS (0.2%, 0.3%, 0.5%, 0.8% and 1.2%). Each square point is a mean value obtained from CDF fit to the measured CCN efficiency spectra corresponding to the mobility diameter. The solid lines are the cumulative distribution fits and error bars are the upper and lower quartiles (25th and 75th).

fractions during winter time. In contrast to this study, Table 2 shows similar study suggesting bigger particles to be more heterogeneous as they are more affected by SOA condensation, coagulation and long range transport compared to smaller particles (Cerully et al., 2011).

The averaged (size and time) κ_{CCN} value was calculated to be 0.18 ± 0.10 during the sampling period. Overall, κ_{CCN} value at SS = 0.2–0.3% was found to be highest (κ_{CCN} = 0.24) and it decreased with the increase in SS (κ_{CCN} = 0.13). The enhanced mass fraction of NO_3^-, SO_4^{2-} and Cl^- in bigger particles (D > 80 nm) made them more hygroscopic compared to smaller particles (Fig. 3). However, less hygroscopic particles at lower size range might have originated from nucleation, biomass burning, vehicular emission and condensation of less oxygenated non/low-volatile organic species (Dusek et al., 2010; Wiedensohler et al., 2009) On the other hand, Bougiatioti et al. (2011) found smaller particles to be more hygroscopic because of more sulfate condensation on them (Table 2). This variation in κ with particle size suggested that bulk κ values can not be a representative for the complete aerosol size range and especially for smaller particles (<100 nm), κ is a crucial parameter for CCN prediction (Kim et al., 2011). We also observed an increase in $(NH_4)_2SO_4$ mass fraction (0.13–0.18) causing an increase in κ value after Dec. 16 at highest SS = 1.2% suggesting the dominating effect of inorganics enhancement. This increase in sulfate was further supported by back trajectory cluster analysis suggesting its arrival via long range transport.

In comparison to Bhattu and Tripathi (2014), D_p > 50 nm aerosols were less hygroscopic in winter (κ_{CCN} = 0.19) compared to summer (0.25), but more hygroscopic than monsoon (0.14) and spring season (0.10) (Table 2). This could be due to low photochemical activity, presence of relatively less oxidized aerosols and dominance of BBOA in winter compared to summer. The different rate of change of κ with particle size in different seasons also provides an idea on the type of condensing material and oxidation, and ageing processes (Paramonov et al., 2013). A recent study in China by Zhang et al. (2014) also found the accumulation mode (κ = 0.31–0.38) particles to be more hygroscopic than Aitken mode (κ = 0.20–0.34) under background conditions. However, in polluted conditions, coating of freshly emitted biomass burning organic portion onto bigger particles (>100 nm) made them less hygroscopic. Despite of the large surface area to volume ratio offered by smaller particles (60–80 nm), coagulation being the dominant process of particle growth caused them to be more heterogeneous and less hygroscopic. Similar to our case, they also observed no trend and large error bars in κ_{CCN} values with increased diameter. This suggested that the presence of complex chemical composition and diverse mixing state in anthropogenically polluted conditions needs to be accounted during CCN prediction.

The average CCN/CN fraction varied between 0.33 and 0.94 for whole SS range measured. Despite the low hygroscopicity of spring aerosols (κ = 0.10–0.12) than winter aerosols (κ = 0.13–0.23), their higher activation fraction was observed due to the presence of greater modal diameter than activation diameter (Bhattu and Tripathi, 2014). This suggested the dominance of aerosol size distribution over chemical composition. The sensitivity analysis of the predicted CCN concentration obtained under different scenarios using chemical composition (size-resolved/bulk), organics solubility, and internally mixed aerosols was also compared against the measured ones (see supplementary section S6 for more details). We observed the reduction in over-prediction (upto ~25%) for LVOOA as soluble organic scenario.

4.3. Hygroscopicity closure (κ_{AMS} and κ_{CCN})

This section compares the hygroscopicity parameter determined using direct size-resolved CCN measurements (κ_{CCN}) at different SS levels with corresponding values calculated using chemical composition from AMS (κ_{AMS}) at same SS conditions. This comparison explains the effect of change in chemical composition and mixing state on hygroscopicity with respect to particle size. As, κ_{CCN} is more reliable at higher number concentration and κ_{AMS} at higher mass concentration, comparing the results from these two approaches is challenging. However, the agreement between κ_{AMS} and κ_{CCN} at larger diameter range (>90 nm) suggested the suitability of κ from either approach in predicting CCN. On the other hand, differences at smaller diameter reached up to an absolute relative deviation ($|(\kappa_{AMS}-\kappa_{CCN})|/\kappa_{CCN}$) of 188% (Fig. 3).

A strong linear correlation observed between f_{org} and κ_{CCN} at lower SS (higher diameter) explained the reduced deviation between κ_{AMS} and κ_{CCN} at higher diameter. This suggested that κ_{AMS} is suitable for predicting the CCN concentration using κ-Kohler model at lower SS (Fig. 4). Although, the information on aerosol mixing state is still quite important at this SS range as it can result in different κ_{AMS} and κ_{CCN} values for same SS levels (Lance et al., 2013).

Table 2
List of past size-resolved ambient CCN measurements done at different sites.

Sampling location	Diameter scan/SS scan	SS	KCCN	CCN parameters (MAF, σ, σ/D)	Implications
Central Amazonia, AMAZE-08 (Gunthe et al., 2009)	Diameter scan	0.10%–0.82%	0.12–0.20	0.91–1.0, 4.0–11.2, 0.07–0.10	Average κ of 0.3 lead to CCN over-prediction by ~50% whereas constant size-distribution lead to over-estimation by factor of ~4–27.
Taunus observatory, Germany FACE-2005 (Dusek et al., 2010)	Diameter scan	0.07%, 0.33%, 0.49%	NA	NA	During NPF events, CCN activity of <100 nm particles decreased whereas >100 nm remained unaffected.
Finokalia, Crete, FAME07 (Bougiatioti et al., 2011)	SMCA approach, Diameter scan (20–100 nm)	0.2%–0.73%	~0.3–0.45	~0.8–0.95, ~0.2–0.3, NA	Small particles (~40 nm) more hygroscopic than larger ones (~100 nm)
Hyytiala, Finland, EUCAARI (Cerully et al., 2011)	Diameter scan (20–100 nm)	0.1%–1.8%	0.14–0.28	0.9–1.0, 0.09–0.19, NA	Bigger particles (80 nm) were more chemically dispersed than small particles (40 and 60 nm)
North China Plain (Deng et al., 2011)	SS scan	0.056%–0.70%	NA	0.8–1, NA,NA	CCN closure using size-resolved activation ratios over-predicted CCN concentration by ~19%
Beijing, China, CAREBeijing-2006 (Gunthe et al., 2011)	Diameter scan	0.07%–0.86%	0.23–0.46	0.81–0.96, 4.6–12.2, 0.03–0.10	Fresh megacity pollution contained small and less hygroscopic particles and hence less CCN.
Gosan (Jeju Island) and Baengnyeongdo, Korean Peninsula (Kim et al., 2011)	Diameter scan	0.2%, 0.6%, 1.0%	0.5–0.61, 0.28–0.52	NA,NA,NA	Particle hygroscopicity is important in CCN prediction for <100 nm aerosols
Puy-de-Dome station, France (Asmi et al., 2012)	SS scan	0.24%, 0.51%	Summer- 0.29, 0.22 Winter-0.43	-NA-	Positive bias of 5% and 2% is due to simplified chemical composition
North China Plain (Deng et al., 2013)	Diameter scan	0.061%–0.812%	0.08–0.26	0.8–1, NA,NA	Both the methods of size-resolved and bulk activation calculated critical diameter gave closure within ±10%.
Paris, MEGAPOLIS (Jurányi et al., 2013)	Both Diameter scan and SS scan	0.1%–1.0%	0.08–0.24	1, NA, NA	Size-resolved measurements are reliable to determine the aerosol mixing state.
Mexico city, MIRAGE2006 (Lance et al., 2013)	Diameter scan	0.07%–1.15%	0.15–0.42	0.81–1.0, NA,NA	CCN concentrations can be well described by κ_{AMS} or κ_{CCN}
Jungfraujoch, Switzerland, CLACE-6 campaign (Rose et al., 2013)	Diameter scan	0.079%–0.66%	0.23–0.43	0.97–1.02, 10.5–16.4, 0.09–0.20	Mono-disperse CCN measurements are better for calculating the hygroscopicity parameter accurately whereas less suitable for measuring total CCN concentration.
Germany (Wu et al., 2013)	Diameter scan	0.07%–0.38%	0.26–0.46	NA,NA,NA	κ_{CCN} is 30% higher than κ_{HTDMA} due to surface tesion reductions, non-ideality, co-condensation of SVOC's, partial solubility or insolubility.
Xianghe, China, AC^3 Exp (Zhang et al., 2014)	Diameter scan	0.08%–0.80%	0.24–0.32	0.94–0.98, 14–38, 0.17–0.29	Large particles were more hygroscopic than small ones. Long-term measurements are required for heavy pollution regions.
Hyytiala, Finland (Hong et al., 2014)	Diameter scan	0.09%–1.26%	0.12–0.28	NA	Non-volatile material contains some hygroscopic material in addition to BC at 280 °C.
Kanpur, India (Bhattu and Tripathi, 2014)	Diameter scan	0.2%–1.0%	Spring: 0.10–0.12 Summer: 0.19–0.29 Monsoon: 0.10–0.20	(0.95–1.04, 10–29, 0.09–0.32) (0.92–0.94, 10–23, 0.18–0.35) (0.95–0.99, 9–24, 0.16–0.26)	CCN prediction is more sensitive to aerosol size distribution in all seasons whereas highest sensitivity to hygroscopicity in monsoon.

Few earlier studies also observed higher deviations between two derived hygroscopicities at lower diameter and suggested that the low signal-to-noise ratio (SNR) of size-resolved composition and size dependence of both f_{org} and κ_{CCN} were the possible reasons (Gunthe et al., 2009; Rose et al., 2013). On the other hand, Liu et al. (2014) added that overlooking the contribution of WSOCs can also underestimate the hygroscopicity for particles < 150 nm.

$\kappa_{AMS}>\kappa_{CCN}$ for Aitken mode particles (mobility diameter < 90 nm, i.e., SS > 0.3%) was observed. It may likely be due to the reason that the chemical composition of organic and

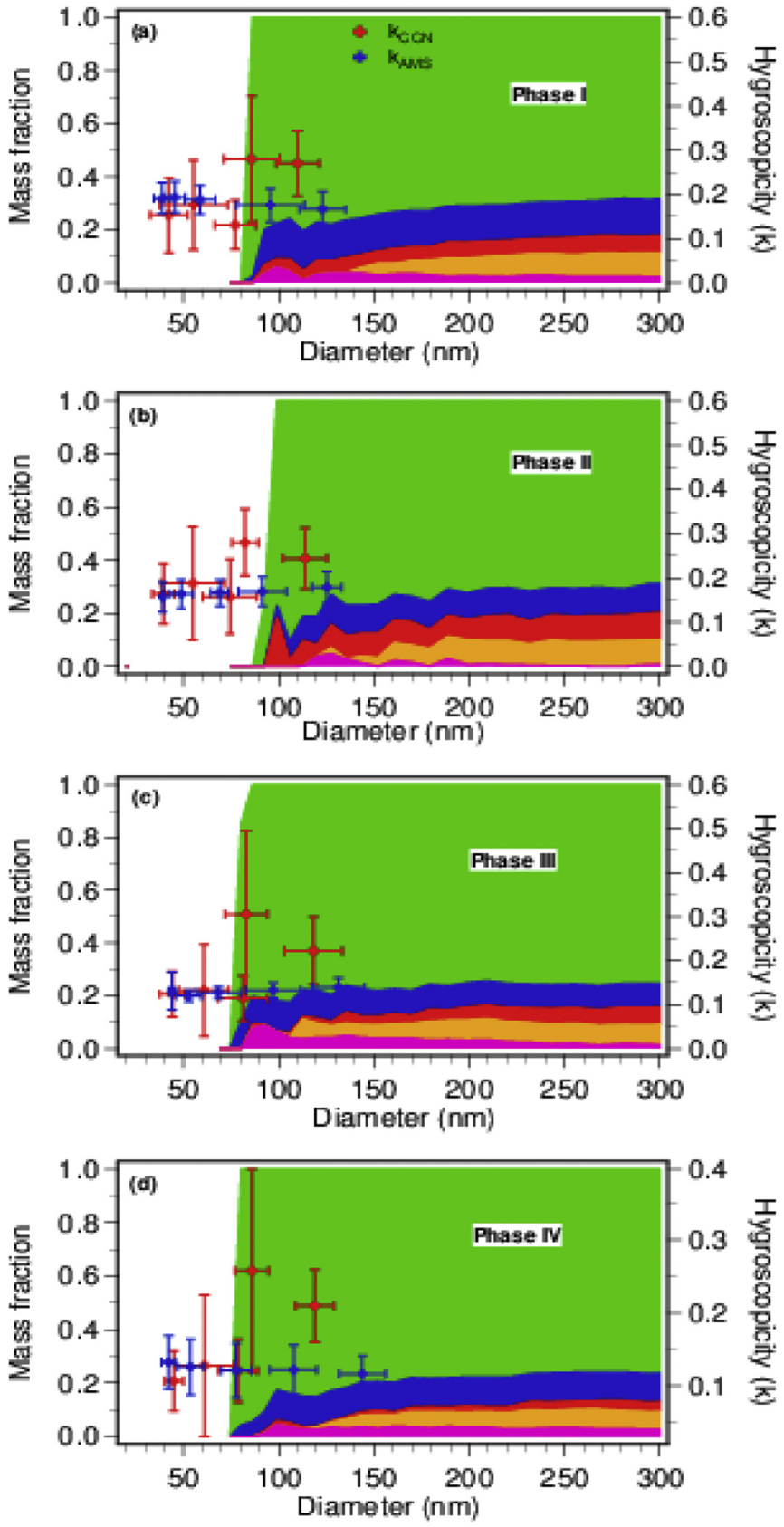

Fig. 3. (a–d) Size-dependent mass fraction of chemical species (Green: Organics, Red: Sulfate, Orange: Ammonium, Blue: Nitrate, Pink: Chloride) measured by the AMS and averaged effective hygroscopicity parameter (κ_{CCN}) with error bars, obtained from size-resolved CCN measurements for different phases (I, II, III, and IV). Light pink markers are the averaged κ_{AMS} values with error bars obtained from the size-resolved chemical composition from AMS.

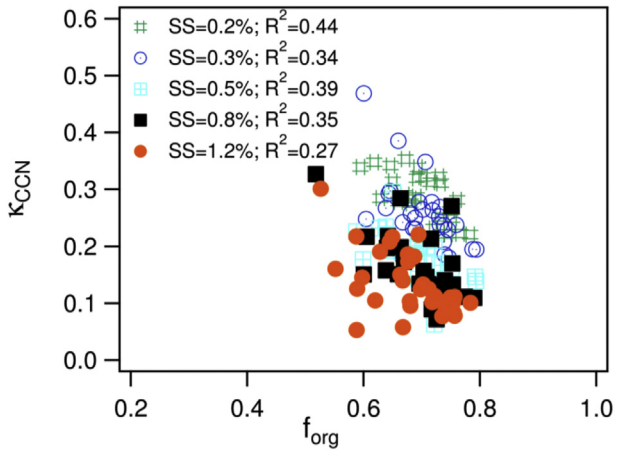

Fig. 4. Correlation between hygroscopicity parameter from size-resolved CCN, κ_{CCN} and organic mass fraction, f_{org} for all SS measured (0.2–1.2%).

inorganic mass present in the Aitken mode was not correctly represented by bulk chemical composition captured by the AMS. Although, Aitken mode is mainly dominated by organic fraction (see Fig. 3) but small changes in inorganic fraction can also add to the total hygroscopicity. However, Gunthe et al. (2011) also observed over-prediction of κ_{AMS} compared to κ_{CCN} in Aitken size range (<100 nm) mainly due to fresh city pollution episodes. CCN prediction was observed to be highly sensitive at lower SS possibly due to the occurrence of steep slopes at the large activation diameters and strong effect of externally mixed CCN-inactive aerosols (Gunthe et al., 2009). However, at lowest SS = 0.2% (i.e., highest size range), $\kappa_{CCN}>\kappa_{AMS}$ was observed for phase II only, which could be due to the presence of externally mixed organic aerosols which does not affect CCN-active aerosol population. In contrast to these results, Lance et al. (2013) observed $\kappa_{AMS}>\kappa_{CCN}$ at higher diameter while $\kappa_{CCN}>\kappa_{AMS}$ at lower diameter. They suggested that the former could be due to the presence of refractory aerosols which were not measured by AMS while latter could be due to the presence of externally mixed organic aerosols which were not CCN active. Among the four phases reported in this study, the error bars in mobility diameter and hygroscopicity as well as the differences between κ_{CCN} and κ_{AMS} were relatively smaller in phase II because of the lower BC concentration and presence of internally mixed aerosols compared to phase I and III (Fig. 3b).

4.4. A case study: effect of biomass burning aerosols on aerosol properties

Fig. 5 shows the time series of CDF parameters obtained at all SS (0.2–1.2%) during the sampling period. The change in these CDF

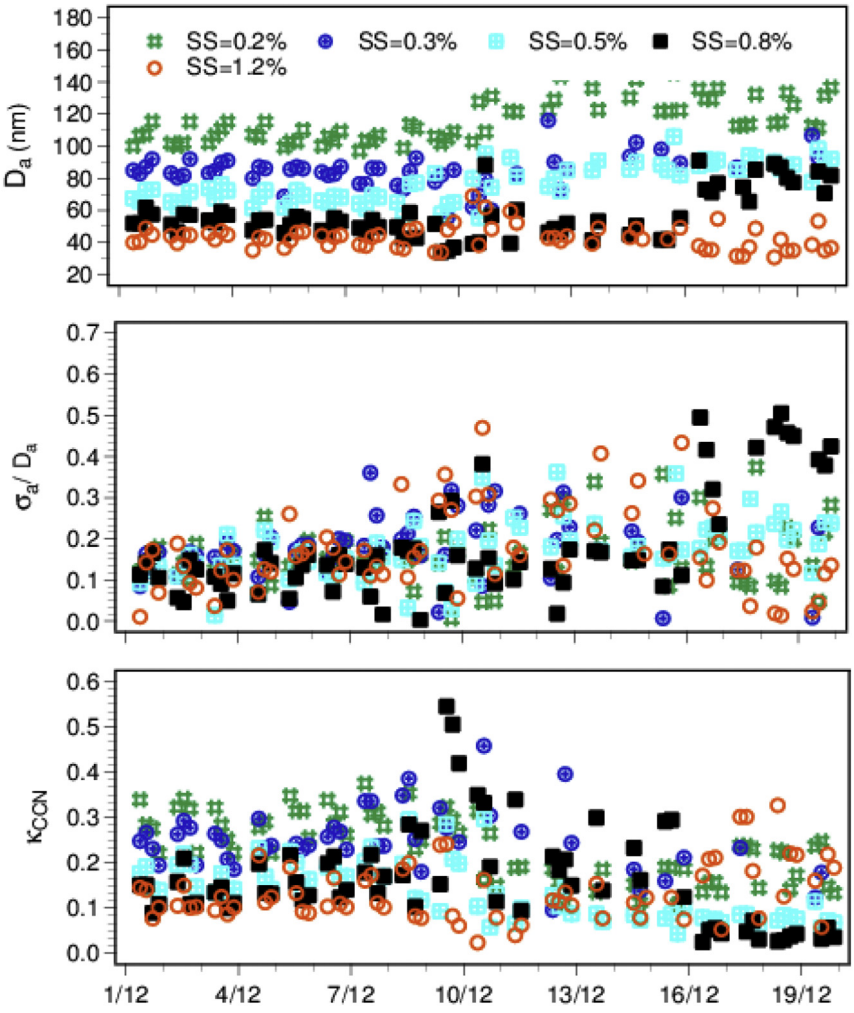

Fig. 5. Time series of the CDF parameters calculated from size resolved CCN measurements at different SS (0.2–1.2%): D_a (activation diameter, nm).

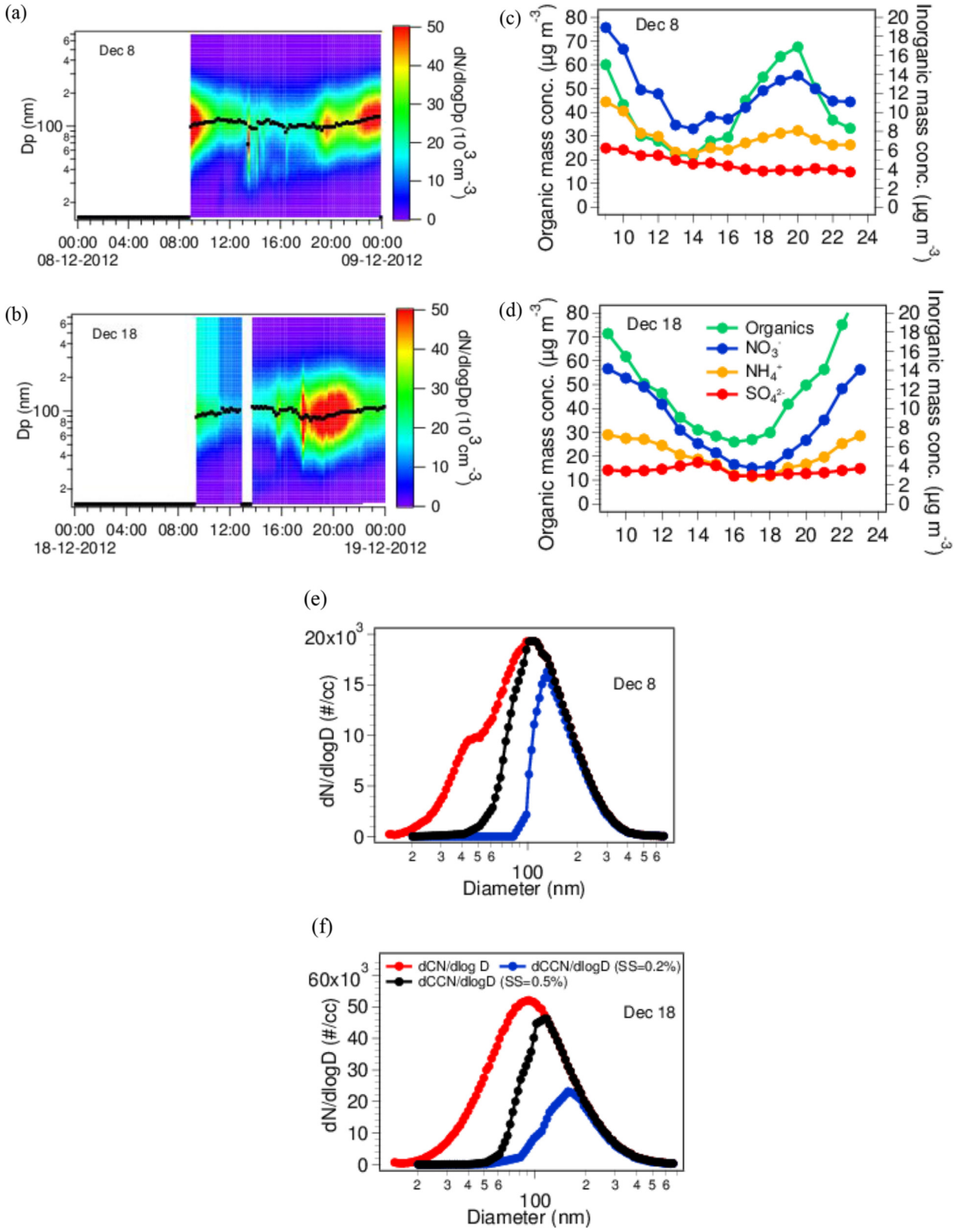

Fig. 6. Diurnal variation of aerosol physical and chemical properties on biomass burning event (Dec 18th) and Dec 8th. (a) and (b) aerosol size distribution, (c) and (d) Bulk chemical composition, and (e) and (f) CCN and CN size distribution.

parameters after Dec 8 was accompanied by a decrease in the total aerosol loading, total organic (f_{org}) and LVOOA fraction, and an increase in BBOA-3 fraction (Fig. 1c, g, and e). A biomass burning event was observed on Dec 18 when BBOA-2 fraction (least oxidized BBOA) increased by ~35% and all the aerosol properties just got reversed of the conventional trend. This event was also

found to be influenced by long range transported biomass burning aerosols (increased BBOA-3 fraction), which was confirmed by back trajectory cluster analysis. To investigate the effect of biomass burning aerosols on CCN activity and hygroscopic properties, more detailed analysis was done. Dec 8 was chosen to be the representative of the conventional trend of the whole period with less BBOA concentration otherwise adjacent days also had long range transported BBOA (BBOA-3) which will not represent the clear impact of local BBOA.

Fig. 6 shows the difference in the properties of aerosols measured on Dec 8 and 18. The activation diameter (D_a) and heterogeneity parameter (σ_a/D_a) increased during the biomass burning event. The difference in D_a ranged between 10 and 44% and decreased with increasing SS. The observed change was higher at SS < 0.8 while it decreased at SS ≥ 0.8. Similar pattern of increase in the activation diameter at lower SS (<0.4) during pollution events bringing fresh biomass burning aerosols and some aged aerosols was observed by Zhang et al. (2014). During this event, the heterogeneity parameter increased with increasing SS (4–44%) suggesting that small particles were more heterogeneous than bigger particles. In addition, hygroscopicity parameter (κ) was also observed to decrease by 4–40%.

On Dec 8, the aerosol concentration showed a peak in the morning (20,000 cm^{-3}) and night (25,000 cm^{-3}) due to traffic emission and lower boundary layer height (Fig. 6a). However, an opposite pattern was observed on Dec 18 with an increase in total aerosol number concentration from 16:00 h and reached a maximum around 18:00 h (35,000 cm^{-3}). The increase in BBOA-2 fraction along with a shift in mode diameter from 100 nm to ~80 nm suggested an inflow of local freshly emitted biomass burning aerosols on Dec 18 (Fig. 6b). Also, the decrease in the slope of f_{BBOA} vs f_{44} by a factor of 1.5 suggested the influence of freshly emitted BBOA on oxidized form of the species (Fig. S3). The bulk aerosol chemical composition obtained from AMS showed the regular diurnal pattern (minima during daytime) on Dec 8 while sudden increase in the concentration of all species except SO_4^{2-} was observed persistently on Dec 18. The concentration of organics, NO_3^- and NH_4^+ reached from 30 to 70 μg m^{-3}, 8–14 μg m^{-3} and 3–7 μg m^{-3}, respectively.

For the same temperature (~20 °C), RH was found to be less on Dec 18 (RH = 40%) compared to Dec 8 (RH = 60%) probably resulting in less effective condensation of secondary hygroscopic species at lower RH conditions during daytime (Seinfeld et al., 2001). The decrease in the average O:C ratio from 0.65 to 0.37 suggested less oxidized organic aerosols on Dec 18 compared to Dec 8. This was further confirmed by the presence of large BBOA-2 fraction (least oxidized) compared to Dec 18. BBOA-3 fraction was also found to be higher on Dec 18 because of the influx of long range transported aerosols from cluster 4 and 6 air mass.

The change in the activation diameter is shown through CCN size distribution (Fig. 6e, f), which was much steeper on Dec 8 at both SS compared to Dec 18 demonstrating lower activation diameter for CCN activation. The activation fraction also reduced from 0.42 to 0.3 and 0.66 to 0.55 for SS = 0.2% and 0.5%, respectively. Also, $\kappa_{AMS}>\kappa_{CCN}$ was observed and the relative difference in κ_{AMS} and κ_{CCN} increased from 97% (Dec 8) to 200% (Dec 18) at lower SS (0.2%). It increased with the increase in SS values suggesting the presence of more CCN-inactive internally mixed aerosols at lower diameter range (<100 nm). This also suggested that a sudden inflow of biomass burning aerosols can suppress the hygroscopic growth of aerosols.

5. Conclusions

This study presents the size-resolved CCN activity measurements in the size range of 20–280 nm made at SS = 0.2–1.2% during December 2012 at Kanpur, India. Smaller particles were observed to be more heterogeneous and less hygroscopic in nature. The deviation between hygroscopicities derived from two different approaches was possibly occurred due to an inappropriate approximation of organic and inorganic mass present in the Aitken mode based on bulk chemical composition and size-resolved fractional contribution of oxidized OA. However, the weak correlation between f_{org} and κ_{CCN} at higher SS explained the larger differences between κ_{CCN} and κ_{AMS}. This suggested that κ_{AMS} can be used to predict the CCN concentration at lower SS conditions reliably with more additional information on mixing state. Further, the assumption of pure internally mixed aerosol does not completely hold true for an anthropogenically polluted site, i.e., Kanpur.

Despite of the large deviation between κ_{CCN} and κ_{AMS} at higher SS, the sensitivity tests of CCN prediction showed better closure results suggesting lesser impact of chemical composition and organic solubility at higher SS. However, at lower SS, results are less robust because of the uncertainty due to the presence of externally mixed CCN-inactive aerosols, higher variability in activation ratios, and less CCN concentration. Later, a case study on the effect of biomass burning aerosols on CCN activity and water uptake characteristics showed increase in D_a by 10–44% and σ_a/D_a by 4–44%, and decrease in κ by 4–40%. However, these observed changes decreased with the increase in SS. This elucidated the negative impact of increased biomass burning aerosol fraction on aerosol growth.

Overall, these results show that the size-resolved CCN measurements are crucial to improve our understanding of the effect of mixing state and chemical composition on CCN activity and should be employed in developing hygroscopicity based CCN parameterization schemes to be involved in climate models.

Acknowledgements

The authors acknowledge the support of IIT Kanpur for providing us HR-ToF-AMS for PG research and teaching. We also acknowledge the partial support through the U.S. Agency for International Development (USAID), Department of Science and Technology (DST), India under Climate Change Program and Indian Institute of Tropical Meteorology (IITM) project funded by Ministry of Earth Sciences (MoES). We gratefully acknowledge the financial support given by the Earth System Science Organization, Ministry of Earth Sciences, Government of India (Grant no. MM/NERC-MoES-03/2014/002) to conduct this research under Monsoon Mission. Acknowledge. We are thankful to Virender Sethi for providing SMPS system to conduct aerosol-size distribution measurements. We acknowledge the NOAA Air Resources Laboratory (ARL) for the provision of the HYSPLIT transport and dispersion model and the READY website (http://ready.arl.noaa.gov) used in this study.

Appendix A. Supplementary data

Supplementary data related to this article can be found at http://dx.doi.org/10.1016/j.atmosenv.2016.07.032.

References

Adachi, K., Buseck, P.R., 2008. Internally mixed soot, sulfates, and organic matter in aerosol particles from Mexico City. Atmos. Chem. Phys. 8, 6469–6481.

Anttila, T., Brus, D., Jaatinen, A., Hyvärinen, A.P., Kivekäs, N., Romakkaniemi, S., Komppula, M., Lihavainen, H., 2012. Relationships between particles, cloud condensation nuclei and cloud droplet activation during the third Pallas Cloud Experiment. Atmos. Chem. Phys. 12, 11435–11450.

Asmi, E., Freney, E., Hervo, M., Picard, D., Rose, C., Colomb, A., Sellegri, K., 2012. Aerosol cloud activation in summer and winter at puy-de-Dôme high altitude site in France. Atmos. Chem. Phys. 12, 11589–11607.

Bauer, S.E., Menon, S., 2012. Aerosol direct, indirect, semidirect, and surface albedo effects from sector contributions based on the IPCC AR5 emissions for preindustrial and present-day conditions. J. Geophys. Res. Atmos. 117, D01206. http://dx.doi.org/10.1029/2011JD016816.

Bhattu, D., Tripathi, S.N., 2014. Inter-seasonal variability in size-resolved CCN properties at Kanpur, India. Atmos. Environ. 85, 161–168.

Bhattu, D., Tripathi, S.N., 2015. CCN closure study: effects of aerosol chemical composition and mixing state. J. Geophys. Res. Atmos. 120, 766–783.

Bougiatioti, A., Nenes, A., Fountoukis, C., Kalivitis, N., Pandis, S.N., Mihalopoulos, N., 2011. Size-resolved CCN distributions and activation kinetics of aged continental and marine aerosol. Atmos. Chem. Phys. 11, 8791–8808.

Cerully, K.M., Raatikainen, T., Lance, S., Tkacik, D., Tiitta, P., Petäjä, T., Ehn, M., Kulmala, M., Worsnop, D.R., Laaksonen, A., Smith, J.N., Nenes, A., 2011. Aerosol hygroscopicity and CCN activation kinetics in a boreal forest environment during the 2007 EUCAARI campaign. Atmos. Chem. Phys. 11, 12369–12386.

Chakraborty, A., Bhattu, D., Gupta, T., Tripathi, S.N., Canagaratna, M.R., 2015. Real-time measurements of ambient aerosols in a polluted Indian city: Sources, characteristics, and processing of organic aerosols during foggy and nonfoggy periods. J. Geophys. Res. Atmos. 120, 9006–9019. http://dx.doi.org/10.1002/2015JD023419.

Dall'Osto, M., Harrison, R.M., Coe, H., Williams, P.I., Allan, J.D., 2009. Real time chemical characterization of local and regional nitrate aerosols. Atmos. Chem. Phys. 9, 3709–3720.

DeCarlo, P.F., Kimmel, J.R., Trimborn, A., Northway, M.J., Jayne, J.T., Aiken, A.C., Gonin, M., Fuhrer, K., Horvath, T., Docherty, K.S., Worsnop, D.R., Jimenez, J.L., 2006. Field-deployable, high-resolution, time-of-flight aerosol mass spectrometer. Anal. Chem. 78, 8281–8289.

Deng, Z.Z., Zhao, C.S., Ma, N., Liu, P.F., Ran, L., Xu, W.Y., Chen, J., Liang, Z., Liang, S., Huang, M.Y., Ma, X.C., Zhang, Q., Quan, J.N., Yan, P., Henning, S., Mildenberger, K., Sommerhage, E., Schäfer, M., Stratmann, F., Wiedensohler, A., 2011. Size-resolved and bulk activation properties of aerosols in the North China Plain. Atmos. Chem. Phys. 11, 3835–3846.

Deng, Z.Z., Zhao, C.S., Ma, N., Ran, L., Zhou, G.Q., Lu, D.R., Zhou, X.J., 2013. An examination of parameterizations for the CCN number concentration based on in situ measurements of aerosol activation properties in the North China Plain. Atmos. Chem. Phys. 13, 6227–6237.

Dusek, U., Frank, G.P., Curtius, J., Drewnick, F., Schneider, J., Kürten, A., Rose, D., Andreae, M.O., Borrmann, S., Pöschl, U., 2010. Enhanced organic mass fraction and decreased hygroscopicity of cloud condensation nuclei (CCN) during new particle formation events. Geophys. Res. Lett. 37 (n/a-n/a).

Farmer, D.K., Cappa, C.D., Kreidenweis, S.M., 2015. Atmospheric processes and their controlling influence on cloud condensation nuclei activity. Chem. Rev. 115, 4199–4217.

Fors, E.O., Swietlicki, E., Svenningsson, B., Kristensson, A., Frank, G.P., Sporre, M., 2011. Hygroscopic properties of the ambient aerosol in southern Sweden – a two year study. Atmos. Chem. Phys. 11, 8343–8361.

Frank, G.P., Dusek, U., Andreae, M.O., 2006. Technical note: a method for measuring size-resolved CCN in the atmosphere. Atmos. Chem. Phys. Discuss. 6, 4879–4895.

Garg, S., Chandra, B.P., Sinha, V., Sarda-Esteve, R., Gros, V., Sinha, B., 2016. Limitation of the use of the absorption angstrom exponent for source apportionment of equivalent black carbon: a case study from the North West Indo-gangetic plain. Environ. Sci. Technol. 50, 814–824.

Gunthe, S.S., King, S.M., Rose, D., Chen, Q., Roldin, P., Farmer, D.K., Jimenez, J.L., Artaxo, P., Andreae, M.O., Martin, S.T., Pöschl, U., 2009. Cloud condensation nuclei in pristine tropical rainforest air of Amazonia: size-resolved measurements and modeling of atmospheric aerosol composition and CCN activity. Atmos. Chem. Phys. 9, 7551–7575.

Gunthe, S.S., Rose, D., Su, H., Garland, R.M., Achtert, P., Nowak, A., Wiedensohler, A., Kuwata, M., Takegawa, N., Kondo, Y., Hu, M., Shao, M., Zhu, T., Andreae, M.O., Pöschl, U., 2011. Cloud condensation nuclei (CCN) from fresh and aged air pollution in the megacity region of Beijing. Atmos. Chem. Phys. 11, 11023–11039.

Hong, J., Häkkinen, S.A.K., Paramonov, M., Äijälä, M., Hakala, J., Nieminen, T., Mikkilä, J., Prisle, N.L., Kulmala, M., Riipinen, I., Bilde, M., Kerminen, V.M., Petäjä, T., 2014. Hygroscopicity, CCN and volatility properties of submicron atmospheric aerosol in a boreal forest environment during the summer of 2010. Atmos. Chem. Phys. 14, 4733–4748. http://dx.doi.org/10.5194/acp-14-4733-2014.

Jacobson, M.Z., 2001. Strong radiative heating due to the mixing state of black carbon in atmospheric aerosols. Nature 409, 695–697.

Jurányi, Z., Tritscher, T., Gysel, M., Laborde, M., Gomes, L., Roberts, G., Baltensperger, U., Weingartner, E., 2013. Hygroscopic mixing state of urban aerosol derived from size-resolved cloud condensation nuclei measurements during the MEGAPOLI campaign in Paris. Atmos. Chem. Phys. 13, 6431–6446. http://dx.doi.org/10.5194/acp-13-6431-2013.

Kanawade, V.P., Tripathi, S.N., Bhattu, D., Shamjad, P.M., 2014. Sub-micron particle number size distributions characteristics at an urban location, Kanpur, in the Indo-Gangetic Plain. Atmos. Res. 147–148, 121–132.

Kim, J.H., Yum, S.S., Shim, S., Yoon, S.C., Hudson, J.G., Park, J., Lee, S.J., 2011. On aerosol hygroscopicity, cloud condensation nuclei (CCN) spectra and critical supersaturation measured at two remote islands of Korea between 2006 and 2009. Atmos. Chem. Phys. 11, 12627–12645.

Kuwata, M., Zorn, S.R., Martin, S.T., 2012. Using Elemental Ratios to Predict the Density of Organic Material Composed of Carbon, Hydrogen, and Oxygen. Environ. Sci. Technol. 46 (2), 787–794. http://dx.doi.org/10.1021/es202525q.

Lance, S., Raatikainen, T., Onasch, T.B., Worsnop, D.R., Yu, X.Y., Alexander, M.L., Stolzenburg, M.R., McMurry, P.H., Smith, J.N., Nenes, A., 2013. Aerosol mixing state, hygroscopic growth and cloud activation efficiency during MIRAGE 2006. Atmos. Chem. Phys. 13, 5049–5062.

Liu, H.J., Zhao, C.S., Nekat, B., Ma, N., Wiedensohler, A., van Pinxteren, D., Spindler, G., Müller, K., Herrmann, H., 2014. Aerosol hygroscopicity derived from size-segregated chemical composition and its parameterization in the North China Plain. Atmos. Chem. Phys. 14, 2525–2539.

McMurry, P.H., Litchy, M., Huang, P.-F., Cai, X., Turpin, B.J., Dick, W.D., Hanson, A., 1996. Elemental composition and morphology of individual particles separated by size and hygroscopicity with the TDMA. Atmos. Environ. 30, 101–108.

Middlebrook, A.M., Bahreini, R., Jimenez, J.L., Canagaratna, M.R., 2011. Evaluation of composition-dependent collection efficiencies for the aerodyne aerosol mass spectrometer using field data. Aerosol Sci. Technol. 46, 258–271.

Mochida, M., Nishita-Hara, C., Kitamori, Y., Aggarwal, S.G., Kawamura, K., Miura, K., Takami, A., 2010. Size-segregated measurements of cloud condensation nucleus activity and hygroscopic growth for aerosols at Cape Hedo, Japan, in spring 2008. J. Geophys. Res. Atmos. 115, D21207. http://dx.doi.org/10.1029/2009JD013216.

Murphy, D.M., Cziczo, D.J., Froyd, K.D., Hudson, P.K., Matthew, B.M., Middlebrook, A.M., Peltier, R.E., Sullivan, A., Thomson, D.S., Weber, R.J., 2006. Single-particle mass spectrometry of tropospheric aerosol particles. J. Geophys. Res. Atmos. 111, D23S32. http://dx.doi.org/10.1029/2006JD007340.

Nandy, B., Sharma, G., Garg, S., Kumari, S., George, T., Sunanda, Y., Sinha, B., 2015. Recovery of consumer waste in India – a mass flow analysis for paper, plastic and glass and the contribution of households and the informal sector. Resour. Conserv. Recycl. 101, 167–181.

Paramonov, M., Aalto, P.P., Asmi, A., Prisle, N., Kerminen, V.M., Kulmala, M., Petäjä, T., 2013. The analysis of size-segregated cloud condensation nuclei counter (CCNC) data and its implications for cloud droplet activation. Atmos. Chem. Phys. 13, 10285–10301.

Peng, J., Hu, M., Guo, S., Du, Z., Zheng, J., Shang, D., Levy Zamora, M., Zeng, L., Shao, M., Wu, Y.-S., Zheng, J., Wang, Y., Glen, C.R., Collins, D.R., Molina, M.J., Zhang, R., 2016. Markedly enhanced absorption and direct radiative forcing of black carbon under polluted urban environments. Proc. Natl. Acad. Sci. 113, 4266–4271.

Petters, M.D., Kreidenweis, S.M., 2007. A single parameter representation of hygroscopic growth and cloud condensation nucleus activity. Atmos. Chem. Phys. 7, 1961–1971.

Petters, M.D., Prenni, A.J., Kreidenweis, S.M., DeMott, P.J., 2007. On Measuring the critical diameter of cloud condensation nuclei using mobility selected aerosol. Aerosol Sci. Technol. 41, 907–913.

Pöschl, U., Martin, S.T., Sinha, B., Chen, Q., Gunthe, S.S., Huffman, J.A., Borrmann, S., Farmer, D.K., Garland, R.M., Helas, G., Jimenez, J.L., King, S.M., Manzi, A., Mikhailov, E., Pauliquevis, T., Petters, M.D., Prenni, A.J., Roldin, P., Rose, D., Schneider, J., Su, H., Zorn, S.R., Artaxo, P., Andreae, M.O., 2010. Rainforest aerosols as biogenic nuclei of clouds and precipitation in the amazon. Science 329, 1513–1516.

Rose, D., Gunthe, S.S., Mikhailov, E., Frank, G.P., Dusek, U., Andreae, M.O., Pöschl, U., 2008. Calibration and measurement uncertainties of a continuous-flow cloud condensation nuclei counter (DMT-CCNC): CCN activation of ammonium sulfate and sodium chloride aerosol particles in theory and experiment. Atmos. Chem. Phys. 8, 1153–1179.

Rose, D., Nowak, A., Achtert, P., Wiedensohler, A., Hu, M., Shao, M., Zhang, Y., Andreae, M.O., Pöschl, U., 2010. Cloud condensation nuclei in polluted air and biomass burning smoke near the mega-city Guangzhou, China – Part 1: size-resolved measurements and implications for the modeling of aerosol particle hygroscopicity and CCN activity. Atmos. Chem. Phys. 10, 3365–3383.

Rose, D., Gunthe, S.S., Jurányi, Z., Gysel, M., Frank, G.P., Schneider, J., Curtius, J., Pöschl, U., 2013. Size-resolved and integral measurements of cloud condensation nuclei (CCN) at the high-alpine site Jungfraujoch. Atmos. Chem. Phys. Discuss. 13, 32575–32624.

Seinfeld, J.H., Erdakos, G.B., Asher, W.E., Pankow, J.F., 2001. Modeling the Formation of Secondary Organic Aerosol (SOA). 2. The predicted effects of relative humidity on aerosol formation in the α-Pinene-, β-Pinene-, Sabinene-, Δ3-Carene-, and cyclohexene-ozone systems. Environ. Sci. Technol. 35, 1806–1817.

Spracklen, D.V., Carslaw, K.S., Kulmala, M., Kerminen, V.-M., Sihto, S.-L., Riipinen, I., Merikanto, J., Mann, G.W., Chipperfield, M.P., Wiedensohler, A., Birmili, W., Lihavainen, H., 2008. Contribution of particle formation to global cloud condensation nuclei concentrations. Geophys. Res. Lett. 35, L06808.

Stocker, T.F., Qin, D., Plattner, G.-K., Alexander, L.V., Allen, S.K., Bindoff, N.L., Bréon, F.-M., Church, J.A., Cubasch, U., Emori, S., Forster, P., Friedlingstein, P., Gillett, N., Gregory, J.M., Hartmann, D.L., Jansen, E., Kirtman, B., Knutti, R., Krishna Kumar, K., Lemke, P., Marotzke, J., Masson-Delmotte, V., Meehl, G.A., Mokhov, I.I., Piao, S., Ramaswamy, V., Randall, D., Rhein, M., Rojas, M., Sabine, C., Shindell, D., Talley, L.D., Vaughan, D.G., Xie, S.-P., 2013. Technical summary. In: Stocker, T.F., Qin, D., Plattner, G.-K., Tignor, M., Allen, S.K., Doschung, J., Nauels, A., Xia, Y., Bex, V., Midgley, P.M. (Eds.), Climate Change 2013: The Physical Science Basis. Contribution of Working Group I to the Fifth Assessment Report of the Intergovernmental Panel on Climate Change. Cambridge University Press, pp. 33–115. http://dx.doi.org/10.1017/CBO9781107415324.005.

Sueper, D.T., Allan, J., Dunlea, E.J., Crosier, J., Kimmel, J., DeCarlo, P., Aiken, A.C., Jimenez, J.L., 2007. A community software for quality control and analysis of data from the aerodyne time-of-flight aerosol mass spectrometers (ToF-AMS). In: 2007 Annual Conference of the American Association for Aerosol Research, Reno, Nev.

Sun, Y.L., Zhang, Q., Schwab, J.J., Chen, W.N., Bae, M.S., Lin, Y.C., Hung, H.M., Demerjian, K.L., 2011. A case study of aerosol processing and evolution in summer in New York City. Atmos. Chem. Phys. 11, 12737–12750.

Ulbrich, I.M., Canagaratna, M.R., Zhang, Q., Worsnop, D.R., Jimenez, J.L., 2009. Interpretation of organic components from positive matrix Factorization of aerosol mass spectrometric data. Atmos. Chem. Phys. 9, 2891–2918.

Wang, J., Cubison, M.J., Aiken, A.C., Jimenez, J.L., Collins, D.R., 2010. The importance of aerosol mixing state and size-resolved composition on CCN concentration and the variation of the importance with atmospheric aging of aerosols. Atmos. Chem. Phys. 10, 7267–7283.

Wiedensohler, A., Cheng, Y.F., Nowak, A., Wehner, B., Achtert, P., Berghof, M., Birmili, W., Wu, Z.J., Hu, M., Zhu, T., Takegawa, N., Kita, K., Kondo, Y., Lou, S.R., Hofzumahaus, A., Holland, F., Wahner, A., Gunthe, S.S., Rose, D., Su, H., Pöschl, U., 2009. Rapid aerosol particle growth and increase of cloud condensation nucleus activity by secondary aerosol formation and condensation: a case study for regional air pollution in northeastern China. J. Geophys. Res. Atmos. 114 (n/a-n/a).

Wu, Z.J., Poulain, L., Henning, S., Dieckmann, K., Birmili, W., Merkel, M., van Pinxteren, D., Spindler, G., Müller, K., Stratmann, F., Herrmann, H., Wiedensohler, A., 2013. Relating particle hygroscopicity and CCN activity to chemical composition during the HCCT-2010 field campaign. Atmos. Chem. Phys. 13, 7983–7996. http://dx.doi.org/10.5194/acp-13-7983-2013.

Zhang, F., Li, Y., Li, Z., Sun, L., Li, R., Zhao, C., Wang, P., Sun, Y., Liu, X., Li, J., Li, P., Ren, G., Fan, T., 2014. Aerosol hygroscopicity and cloud condensation nuclei activity during the AC3Exp campaign: implications for cloud condensation nuclei parameterization. Atmos. Chem. Phys. 14, 13423–13437.